Nanoscale Advances

ROYAL SOCIETY OF CHEMISTRY

PAPER

View Article Online
View Journal | View Issue

Cite this: *Nanoscale Adv.*, 2021, **3**, 3909

Synergistic effects of Ga doping and Mg alloying over the enhancement of the stress sensitivity of a Ga-doped MgZnO pressure sensor†

Ping Han Lee,‡[a] Sanjaya Brahma,‡[ac] Jit Dutta,[a] Jow-Lay Huang*[abc] and Chuan-Pu Liu *[a]

We demonstrate the synergistic effects of Ga doping and Mg alloying into ZnO on the large enhancement of the piezopotential and stress sensing performance of piezotronic pressure sensors made of Ga-doped MgZnO films. Piezopotential-induced pressure sensitivity was enhanced through the modulation of the Schottky barrier height. Doping with Ga (0.62 Å) of larger ionic radius and alloying with Mg (0.57 Å) of smaller ionic radius than Zn ions can synergistically affect the overall structural, optical and piezoelectric properties of the resulting thin films. The crystal quality of Ga-doped MgZnO films either improved ($X_{Ga} \leqq 0.041$) or deteriorated ($X_{Ga} \geqq 0.041$) depending on the Ga doping concentration. The band gap increased from 3.90 eV for pristine MgZnO to 3.93 eV at $X_{Ga} = 0.076$, and the piezoelectric coefficient (d_{33}) improved from ~23.25 pm V^{-1} to ~33.17 pm V^{-1} at an optimum Ga concentration ($X_{Ga} = 0.027$) by ~2.65 times. The change in the Schottky barrier height $\Delta\Phi_b$ increased from −4.41 meV (MgZnO) to −4.81 meV ($X_{Ga} = 0.027$) and decreased to −3.99 meV at a high Ga doping concentration ($X_{Ga} = 0.041$). The stress sensitivity (0.2 kgf) enhanced from 28.50 MPa^{-1} for the pristine MgZnO to 31.36 MPa^{-1} ($X_{Ga} = 0.027$) and decreased to 25.56 MPa^{-1} at higher Ga doping concentrations, indicating the synergistic effects of Ga doping and Mg alloying over the pressure sensing performance of Ga-doped MgZnO films.

Received 24th December 2020
Accepted 18th May 2021

DOI: 10.1039/d0na01069c

rsc.li/nanoscale-advances

1. Introduction

The pioneering discovery of the theory of piezotronics has led to the fabrication of several interesting nanoelectronic devices, out of which piezotronic sensors[1–3] provide not only ultrahigh sensitivity on minute mechanical vibrations, but also unique self-power capability to generate self-powered stress/strain sensors. By developing semiconducting piezoelectric materials (for example ZnO and GaN), multifunctional piezotronic devices can be advanced by the synergistic effects of semiconducting properties in the form of energy harvesting. The principle of a piezotronic pressure sensor is based on the modulation of the Schottky barrier height (SBH) at the metal–semiconductor interface subject to external stress that polarizes the material and induces piezopotential at the interfaces, where the SBH is dominated by the stress-induced change in the piezoelectric effects. Piezotronic stress sensors are superior to piezo-resistance sensors in terms of low energy consumption and better device performances in response, sensitivity and gauge factor.[1,4]

ZnO is an environmentally benign hexagonal wurtzite piezoelectric-semiconducting material with a non-centrosymmetric crystal structure, where an external stress displaces the centers of the cations, and the anions create a piezopotential in the structure[5] suitable for future electro-mechanical devices. ZnO-based piezotronic strain sensors have been reported based on micro/nanowires,[6] nanobelts,[4] nanowire array,[7] hybrid structures with carbon fiber,[8] and polystyrene hybridized flexible films.[3] Zhang *et al.*[4] demonstrated a high gauge factor of 4036 from the piezotronic strain sensors using In-doped ZnO nanobelts, significantly higher than others[3,8] (references therein). Although pressure sensor devices based on Au nanowires,[9] SnSe nanoplates,[10,11] layered transition metal dichalcogenides,[12] photoresists[13] and graphene[14] have been reported, the piezotronic effect has not been studied. Piezotronic stress sensors based on ZnO micro/nanowires[15] or nanowire arrays[16] have hardly been investigated, and particularly, thin film-based devices have not been examined and are worth investigating.

Doping in ZnO is generally considered as an effective strategy to increase the electrical conductivity,[17–19] engineer the band gap,[20,21] and enhance the piezoelectric coefficient,[22,23] all of

[a]*Department of Materials Science and Engineering, National Cheng Kung University, Tainan 701, Taiwan. E-mail: jlh888@mail.ncku.edu.tw; cpliu@mail.ncku.edu.tw*

[b]*Center for Micro/Nano Science and Technology, National Cheng Kung University, Tainan 70101, Taiwan*

[c]*Hierarchical Green-Energy Materials (Hi-GEM) Research Center, National Cheng Kung University, Tainan 70101, Taiwan*

† Electronic supplementary information (ESI) available. See DOI: 10.1039/d0na01069c

‡ These authors (Sanjaya Brahma, Ping Han Lee) have equal author contributions.

which are essential to boost the overall device functionality. Pan *et al.*[22–24] fabricated Cr-, Fe-, V-substituted ZnO thin films, and achieved high piezoelectric coefficients of 120 pm V^{-1} ($Zn_{1-x}Cr_xO$), 110 pC N^{-1} ($Zn_{1-x}V_xO$) and 110 pC N^{-1} ($Zn_{1-x}Fe_xO$), respectively. Kumar *et al.*[25] reported very high piezoelectric coefficient (420 pm V^{-1}) in Y-doped ZnO nanosheets. Mg incorporation into ZnO has been reported to increase the bandgap (3.3–7.3 eV),[26] in addition to achieving a higher piezoelectric coefficient (54.1 pm V^{-1}) at an Mg concentration of 11.14 at% (ref. 27) as alloying effects. MgZnO films have been investigated extensively as UV photodetectors,[28] where the sensitivity was significantly enhanced by external strain in the realm of piezo-phototronics. For ZnO, each of alloying and doping effect has been demonstrated to be effective to boost the piezoelectric properties. It is worth examining if these two effects can be combined to further enhance the piezoelectric properties by simultaneously incorporating two different types of ions into ZnO. For example, Ga-doped MgZnO (MgZnO:Ga) thin films have been utilized as a transparent conductive oxide,[29–31] but the study on the piezoelectric property has never been reported. Nevertheless, Ga competes with solute atoms of Mg to replace for the same Zn sites. Therefore, while the alloying Mg atoms induce compressive stress, Ga doping generates tensile stress, and the local strain can be mixed by the combined effects. The complexity of doping and alloying atoms in developing functional ternary compounds has never been examined before and is worth examining, not to mention further complexity from various degrees of carriers it induces. Ga is commonly chosen as an n-type dopant for ZnO, where gentle lattice distortion can retain the ZnO high crystal quality with a large tunable carrier concentration. If ions with the size largely deviate from Zn ions, crystal defects tend to form, even resulting in different ferroelectric phases to form. Here, for the first time, we demonstrate the synergistic effects of Ga doping and Mg alloying into ZnO for the enhancement of the piezo-potential over the performance of the MgZnO:Ga film stress sensor.

2. Experimental

MgZnO:Ga thin films were deposited on a p-type (111) Si substrate by an r.f. magnetron co-sputtering system using $Mg_{0.3}Zn_{0.7}O$ (2 inches in diameter) and pure Ga_2O_3 (99.99% purity, 2 inches in diameter) as the targets. Prior to the deposition, the Si substrates were sequentially cleaned in acetone, isopropyl alcohol and deionized water for 10 min *via* ultrasonic agitation. The cleaned substrates were dried by blowing N_2 gas (99.99%) before being inserted into the chamber. The vacuum chamber was pumped down to 4–6 $\times$ 10^{-6} torr; then, Ar and O_2 were introduced into the chamber at the flow rates of 10 and 20 sccm (standard cubic centimeter per minute) to reach the working pressure of 6 $\times$ 10^{-2} torr, respectively. The distances between the substrates and the targets of $Mg_{0.3}Zn_{0.7}O$ and Ga_2O_3 were set at 10 cm and 9 cm, respectively. The pre-sputtering was conducted for about 10 min to establish stability and remove the contaminations (if any) from the surface. The Ga doping concentration in the thin films was varied by varying the applied power to the Ga_2O_3 target but by maintaining a constant power of 100 watt (W) to the $Mg_{0.3}Zn_{0.7}O$ target. During the deposition, the substrate temperature was fixed at 250 °C, and all the film thicknesses were controlled to be around 500 nm by controlling the deposition time.

X-ray diffraction (XRD) (Bruker D8 DISCOVER) and field emission scanning electron microscopy (FESEM) (HITACHI SU-8000) equipped with energy dispersive X-ray spectroscopy (EDS) were utilized to identify the crystallographic orientations, phases, compositions, morphologies and thickness of the $Mg_xZn_{1-x}O$ thin films. Chemical binding energy was investigated by X-ray photoelectron spectroscopy (XPS) (JEOL JAMP-9500F Auger Electron, Japan). Room temperature absorption and transmission spectra were recorded using a UV-Visible-near infrared spectrophotometer (HITACHI U4100). Moreover, piezoelectric constants were obtained *via* piezo-response force microscopy (PFM) of a multi-functional scanning probe microscope (Bruker Dimension ICON).

Metal/semiconductor/metal (MSM) Schottky-type pressure sensors were fabricated based on various MgZnO:Ga films with Au electrodes (0.8 $\times$ 2.8 cm^2) on the front side (film) and back

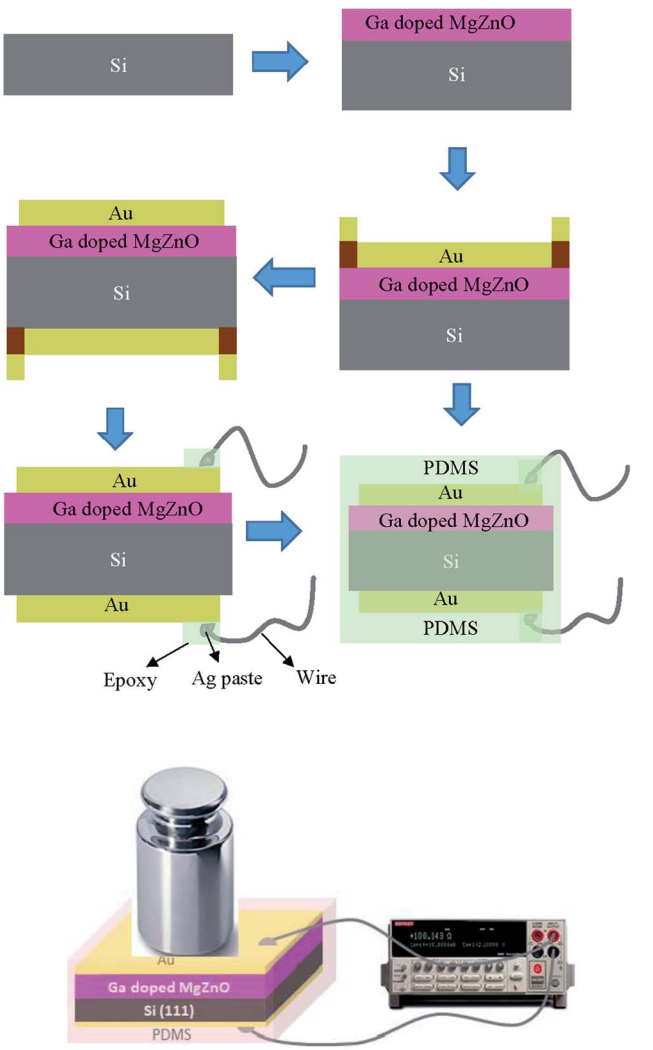

Scheme 1 Schematic diagram of Ga:MgZnO pressure sensor.

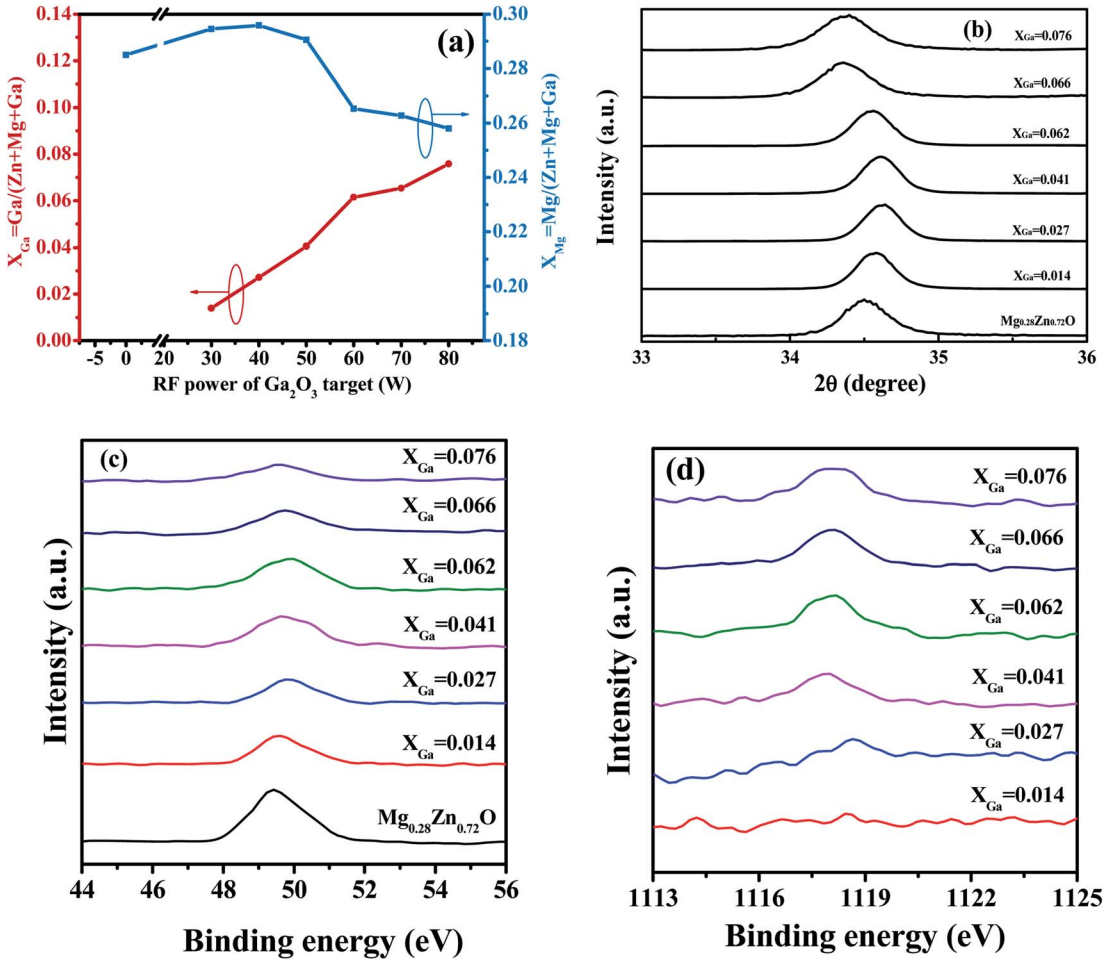

Fig. 1 Ga-doped MgZnO (MgZnO:Ga) thin films. (a) EDX results showing the Ga and Mg content, (b) slow-scan XRD diffraction patterns from 33° to 36°, XPS spectra of (c) Mg 2p and (d) Ga 2p peaks of the MgZnO:Ga thin films.

side (Si substrate) of the device *via* a precision etching and coating system. The wire bonding was done by silver paste, and the devices were packaged by polydimethylsiloxane (PDMS) to prevent from corrosion or oxidation. Stress-dependent *I–V* curves were acquired using a multi-function power meter (Keithley 2400) in a bias voltage ranging from −5 V to +5 V. The stress was applied simply by placing the weights (0.2 kg and 0.5 kg) on the sensor device. The schematic of the device fabrication and the measurement of stress dependent *I–V* curve is shown in Scheme 1.

3. Results and discussion

Fig. 1a shows the EDS results of the pristine MgZnO and various MgZnO:Ga thin films, where X_{Ga} and X_{Mg} are defined as Ga/(Zn + Mg + Ga) (at%) and Mg/(Zn + Mg + Ga) (at%), respectively. The Ga content in the MgZnO:Ga thin films varied from 0.56 at% to 3.19 at% corresponding to X_{Ga} = 0.014–0.076, and the Mg composition varied slightly from 11.59 at% to 10.86 at%, corresponding to X_{Mg} = 0.285–0.258 with an increase in the Ga_2O_3 target power (Table S1, ESI†). It was supposed that the doping of Ga with larger ionic radius (Ga^{3+} = 0.062 nm)[31] creates tensile strain, whereas the Mg (Mg^{2+} = 0.057 nm) incorporation yields compressive strain, and therefore, the opposite effects can be compensated by co-doping for the least lattice deformation. Fig. 1b illustrates the slow scan XRD spectra of numerous MgZnO:Ga thin films showing a highly (0002) preferred orientation without any peaks from Ga_2O_3 or MgO (Fig. S1,† XRD pattern from 2θ = 20–80°). This indicates that all films were made of a pure ZnO wurtzite structure with preferential *c*-axis orientation. Table 1 summarizes the peak position (2θ°), *d*-spacing (Å) and full width at half maximum (FWHM) of the

Table 1 Peak shift and FWHM of the (0002) peak of the Ga-doped MgZnO films

X_{Ga}	0	0.014	0.027	0.041	0.062	0.066	0.076
2θ (°) of the (0002) peak	34.55	34.57	34.62	34.60	34.55	34.37	34.38
d (Å)	2.595	2.594	2.590	2.592	2.595	2.609	2.608
FWHM (2θ°)	0.364	0.323	0.299	0.301	0.318	0.390	0.418

(0002) peaks corresponding to the various Ga doping concentrations. The shift of the (0002) diffraction peak is determined by the competition of larger Ga (0.062 nm) and smaller Mg (0.057 nm) ions than the parent Zn (0.06 nm) ions. The XRD peak initially shifts to a higher angle until $X_{Ga} = 0.027$ (Ga = 1.18 at%, Mg = 12.86 at%), and then, remains almost the same from $X_{Ga} = 0.027$ to $X_{Ga} = 0.041$ (Ga = 1.77 at%, Mg = 12.69 at%). Finally, this peak decreased with further increase in the Ga concentration. When $X_{Ga} < 0.041$, the peak shift is strongly dominated by the high Mg concentration (12.86 at%) compared to Ga (1.18 at%). The incorporation of the smaller Mg ions causes a smaller $d_{(0002)}$ spacing and the peak

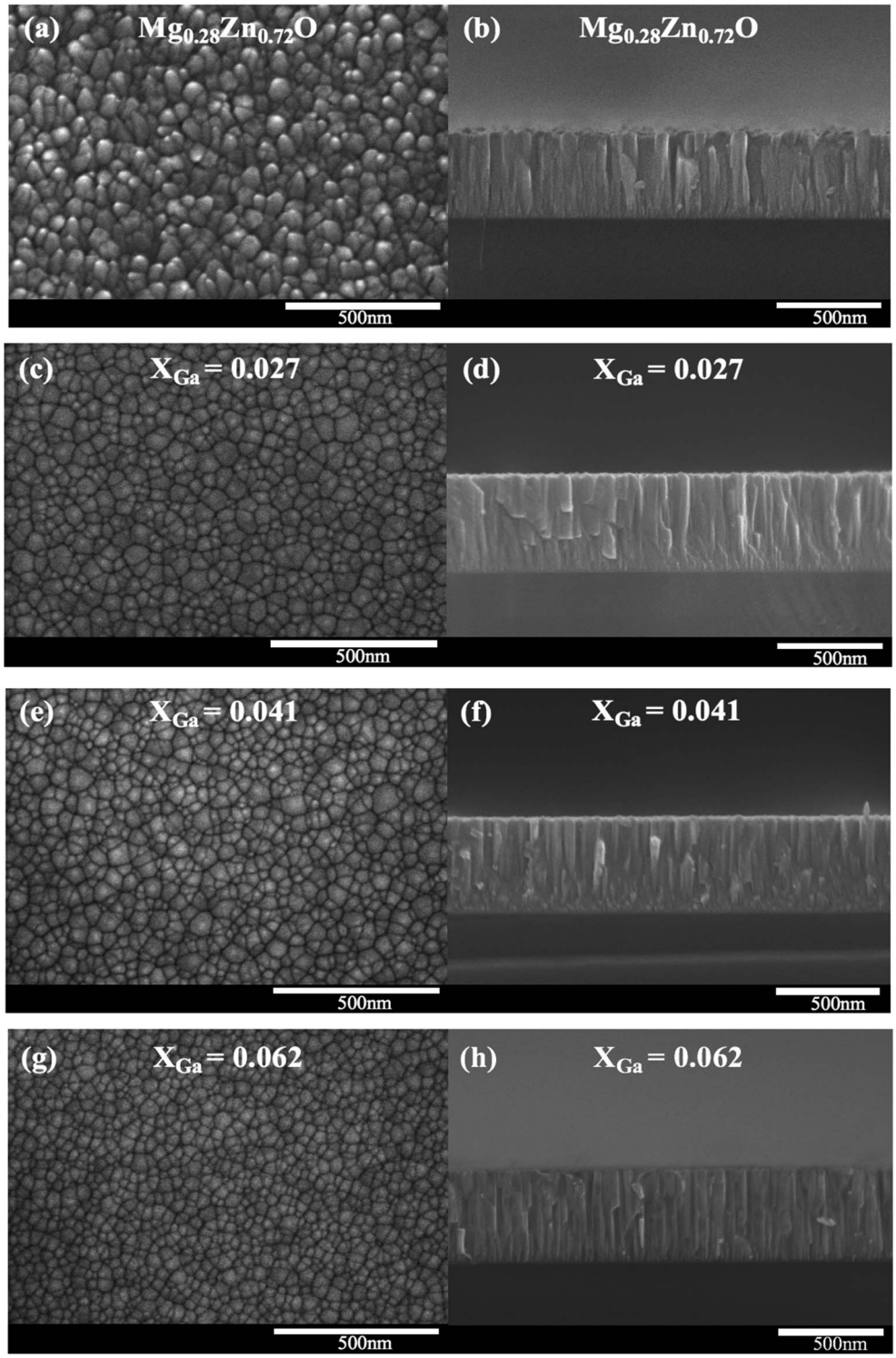

Fig. 2 SEM plan-view and cross-sectional images of the MgZnO:Ga thin films with X_{Ga} = (a, b) 0, (c, d) 0.027, (e, f) 0.041, (g, h) 0.062.

shifted towards higher angles, which agrees well with the previously published report.[32] However, at higher Ga concentrations when $X_{Ga} > 0.041$, the larger Ga ions caused $d_{(0002)}$ to be larger, and the peak shifted towards lower angles. Similarly, the FWHM ($2\theta^{\circ}$) decreased from 0.364 for the undoped MgZnO ($Mg_{0.28}Zn_{0.72}O$) to 0.299 for $X_{Ga} = 0.027$, and then it increased with further increase in the Ga concentration ($X_{Ga} \geqq 0.041$), indicating the combined effects of both Ga doping and Mg alloying over the variation of the crystal size in relation to the least lattice distortion. It implies that the intrinsic compressive strain of the pristine MgZnO film was compensated by the addition of Ga up to $X_{Ga} = 0.027$, causing the narrowing of the (0002) peak; however, tensile strain escalated with the incorporation of more Ga content corresponding to the transition of the (0002) peak shift. The XPS spectra in Fig. 1(c and d) present the variation in the binding energy as well as the intensity of the Mg 2p and Ga 2p peaks of the MgZnO:Ga films with various Ga doping concentrations. The peak corresponding to Mg–O at 49.7 eV shifts towards a higher binding energy (Fig. 1c), and the intensity of the peak gradually decreases with the Ga doping concentration, indicating a decrease in the Mg concentration in the films. Simultaneously, the intensity of the Ga–O binding energy peak at 1117.4 eV increased with the power of the Ga_2O_3 (Fig. 1d) target, and the broad peak was due to the presence of the Ga^{3+} and Ga^{5+} oxidation states.[33]

It can be seen in the plan-view and cross-sectional FESEM images (Fig. 2) that the as-grown MgZnO and various MgZnO:Ga thin films showed an identical morphology with a densely packed columnar microstructure, where the thicknesses of the films were maintained at ~500 nm controlled by the deposition time. The surface of the MgZnO thin film (Fig. 2a) shows a relatively larger grain size, and a regular reduction in the grain size is observed with an increase in the Ga doping concentration. This trend is consistent with the FWHM of the (0002) peak from $X_{Ga} = 0$ to $X_{Ga} = 0.027$. In general, the larger grain size led to a rougher surface, and smaller grain size smoothens the surface. Moreover, the dopants at the surface and grain boundaries might act as surfactants, which decreases the energy at the surface/grain boundary, modifies the diffusion rate of other atoms (Zn, Mg *etc.*), and stabilizes the growth leading to the decrease in the grain size.[34,35] The cross-sectional images also confirmed a gradual modification of the film surface morphology from columnar nanorod-like to film-like, and all films had a (0002) preferential orientation, indicating the suitability of the r.f. sputtering for the deposition of the highly oriented Ga-doped MgZnO thin films.

Fig. 3a depicts the transmittance and bandgap energy of the undoped and various MgZnO:Ga thin films, showing a gradual red-shift for Ga-doped $Mg_xZn_{1-x}O$ films. The band gap (Fig. 3b, and Fig. S2†) of the $Mg_{0.28}Zn_{0.72}O$ film was 3.90 eV, and that increased gradually to 3.93 eV ($X_{Ga} = 0.076$) with the increase in the Ga doping concentration. Fig. 4 shows the piezoelectric coefficient (d_{33}) of numerous MgZnO:Ga films. As compared to the pristine $Mg_{0.28}Zn_{0.72}O$ thin film (d_{33} = 23.25 pm V^{-1}), d_{33} rose gradually to a maximum of 33.17 pm V^{-1} corresponding to the Ga concentration of 1.18 at% ($X_{Ga} = 0.027$) and Mg concentration of 12.86 at% ($X_{Mg} = 0.302$), and then fell. The

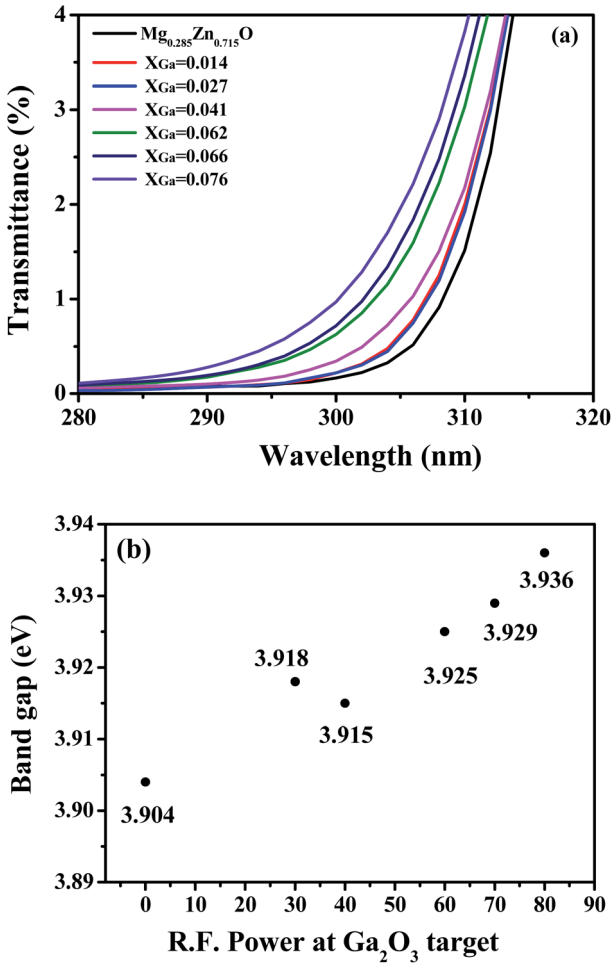

Fig. 3 (a) Transmittance spectra and (b) bandgap energies of the $Mg_{0.28}Zn_{0.72}O$ and various MgZnO:Ga thin films.

detailed calculation of the piezoelectric coefficient from the original data is described in Fig. S3 and Table S2.† The increase in the piezoelectric coefficient is due to the alloying effect from

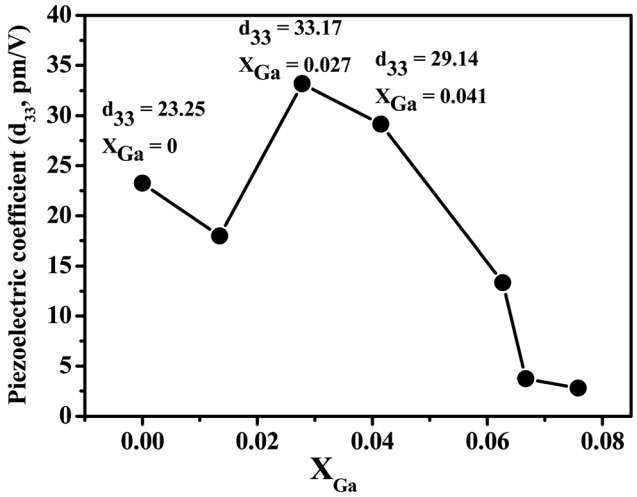

Fig. 4 Piezoresponse force microscopy results of the piezoelectric coefficient of the MgZnO:Ga thin films with Ga concentration.

different electronegativity and solute ionic size of Mg (0.57 Å) compared to the matrix Zn ionic size (0.60 Å); the polarization can be enhanced in the $Mg_xZn_{1-x}O$ ternary compound films,[32] reaching a high piezoelectric coefficient at around Mg = 30 at% for $Mg_{0.3}ZnO_{0.7}O$. This work further unveils the coupling effect of doping effect through Ga donors where Ga of even larger ionic size than Zn can substitute for either Ga or Zn sites with the aforementioned alloying effect can evidently further enhance piezoelectric coefficient (33.17 pm V^{-1}, @$X_{Ga} = 0.027$) at high Mg concentration of 12.86 at% (Table S1†) through bond distortion by the complicated strain field induced by the mixing effect of Ga, Mg and Zn in the same lattices. Wang *et al.*[36] studied the dependence of the doping-induced *c*-axis lattice constant on d_{33} in relation to the piezoelectric stress coefficients (e_{33} and e_{31}) as follows.

$$e_{33} = -2e_{31} = \frac{\sqrt{3}ne}{8b^2} \text{ and } d_{33} = 2e_{31}S_{13}^{E} + e_{33}S_{33}^{E}$$

thus,[36,37]

$$d_{33} = \frac{\sqrt{3}ne}{8b^2}\left(S_{33}^{E} - S_{13}^{E}\right), \quad b = \frac{3}{8}c$$

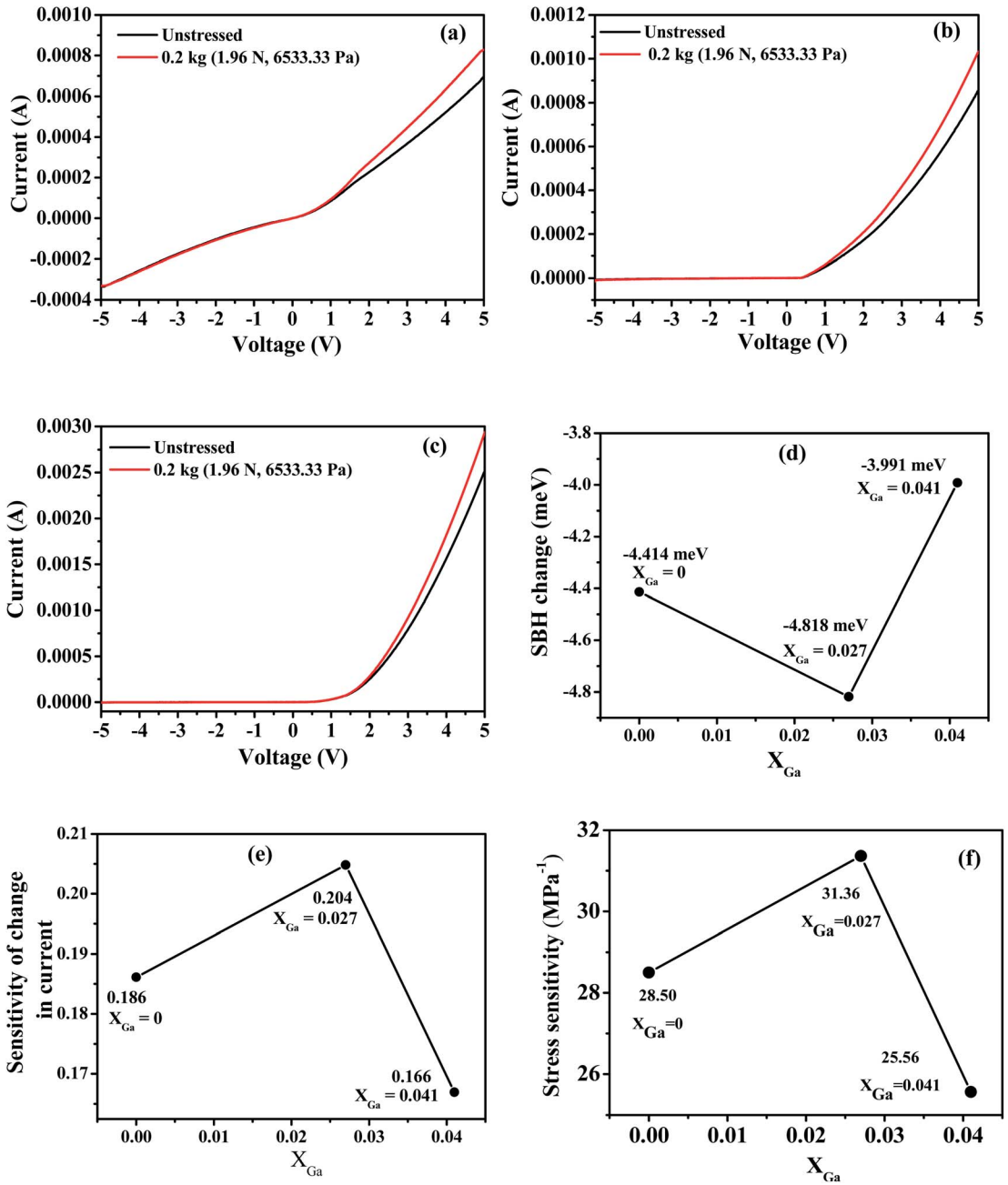

Fig. 5 Unstressed and stressed (0.2 kgf) *I*–*V* characteristics of the piezotronic stress sensors made of MgZnO:Ga films: (a) X_{Ga} = 0 ($Mg_{0.28}Zn_{0.72}O$) (b) X_{Ga} = 0.027 and (c) X_{Ga} = 0.041, with the corresponding (d) SBH change, (e) sensitivity of change in current and (f) stress sensitivity.

where n (=1.32) is the number of equivalent atomic charges, e is the charge of the electron, b is the bond length of ZnO lattice, S_{13}^{E} and S_{33}^{E} are the elastic compliances at the constant electric field of ZnO and c is the lattice parameter. It should be mentioned that the lattice parameter c decreases at low Ga doping concentration up to around $X_{Ga} = 027$, 0.041, and then, shows an increasing trend when $X_{Ga} > 0.041$ (Fig. S4†). Thereby, the enhancement of the piezoelectric coefficient in the Ga-doped MgZnO films may be due to the decrease in c, leading to the shrinkage in the bond length, which facilitates the easy rotation of the non-collinear bonds in the direction of the applied field to produce strain.[23] Furthermore, crystallinity, which increases with the Ga doping concentration (X_{Ga} = 0.027), might be a crucial parameter in increasing the d_{33} value. Here, the optimum Ga-doped MgZnO film achieved the highest piezoelectric coefficient of 33.17 pm V^{-1}, which is much higher than that of the $Mg_{0.28}Zn_{0.72}O$ film (23.25 pm V^{-1}) and pristine ZnO (d_{33} = 12.4 pm V^{-1}). Therefore, the substitution of Ga into MgZnO not only maintains its wide bandgap but also enhances the piezoelectric properties.

Fig. 5 shows the stress sensing properties of the pressure sensor incorporating various MgZnO:Ga thin films through current–voltage (I–V) characteristics with/without the application of stress (Table S3†). All I–V curves (Fig. 5a–c) demonstrated a typical Schottky diode behavior, except for noticeable leakage current found in the MgZnO ($X_{Ga} = 0$)-based device, probably originating from smaller SBH, as evidenced by the trend of the larger turn-on voltage with Ga doping. Nevertheless, high conductivity accompanied by Ga doping can be observed in the current reading under no stress condition, where the current gradually increases from 0.698 mA at 5 V for the undoped MgZnO film to 0.857 mA (X_{Ga} = 0.027), 2.519 mA (X_{Ga} = 0.041) with the increase in the Ga concentration. The piezotronic response is distinct for all devices, in that the applied compressive stress renders the SBH to decrease and the current to increase, where the current change is acquired as 0.698 mA to 0.828 mA for MgZnO, 0.857 mA to 1.032 mA for X_{Ga} = 0.027, and 2.519 mA to 2.939 mA for X_{Ga} = 0.041.

Through the thermionic emission theory, the change in the SBH ($\Delta\Phi_b$) due to the applied stress can be calculated from $\Delta\Phi_b = -\frac{kT}{q}\ln[I(\varepsilon)/I(0)]$, where $I(\varepsilon)$ and $I(0)$ refer to the current reading under stress and no-stress, respectively. $\Delta\Phi_b$ in Fig. 5d increased initially with the Ga doping from −4.41 meV (MgZnO) to −4.81 meV (X_{Ga} = 0.027), and decreased to −3.99 meV at high a Ga doping concentration (X_{Ga} = 0.041). Besides, the sensitivity

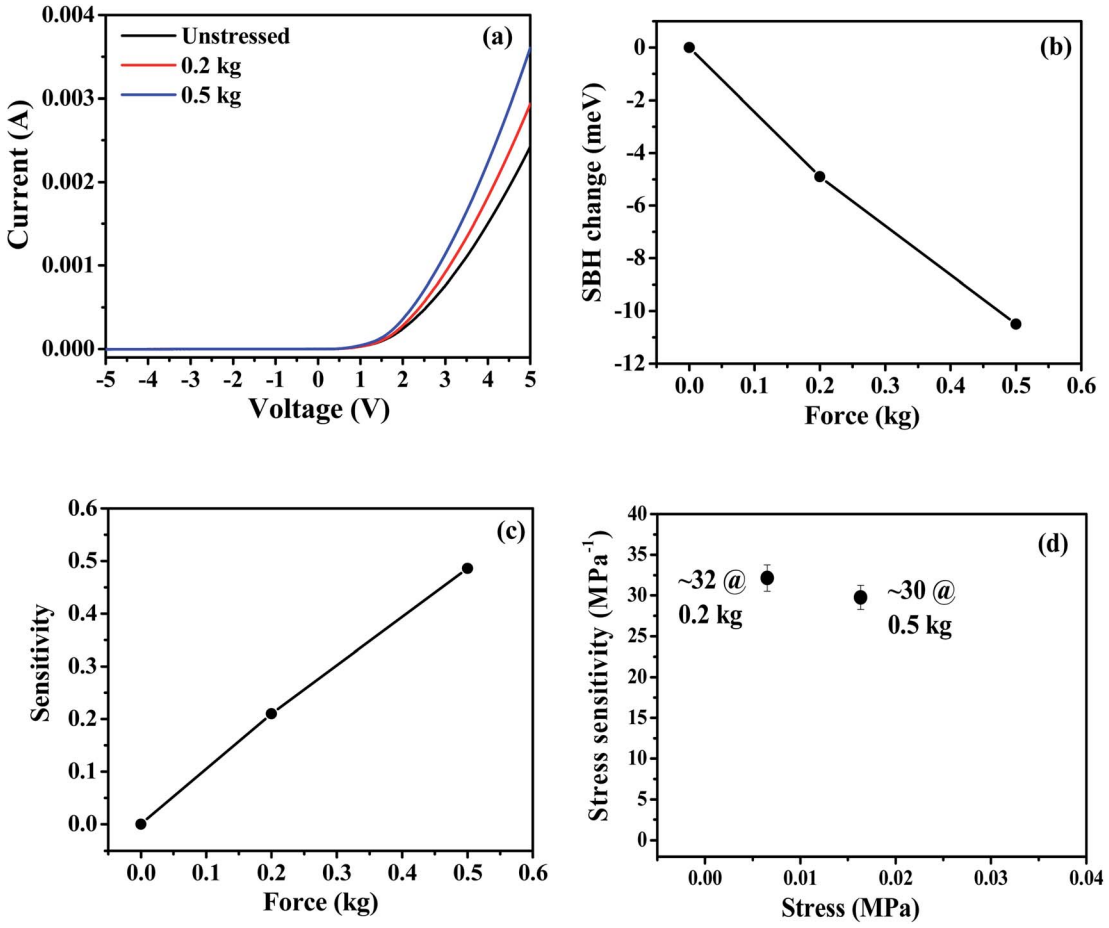

Fig. 6 (a) I–V characteristics, (b) SBH change, (c) sensitivity of the change in current and (d) stress sensitivity of the piezotronic stress sensor made of an MgZnO:Ga (X_{Ga} = 0.041) thin film under various external forces (0.2 kg and 0.5 kg).

of change in current at 0.2 kgf (Fig. 5e), defined as $\frac{\Delta I}{I} = \frac{I(\varepsilon) - I(0)}{I(0)}$ was enhanced from 0.186 for the pristine MgZnO to 0.204 ($X_{Ga} = 0.027$), which decreased to 0.166 at $X_{Ga} = 0.041$. The stress sensitivity (Fig. 5f, Table S4†), as defined by $\frac{\Delta I/I}{\text{stress}}$, increased from 28.50 MPa^{-1} ($X_{Ga} = 0$) to 31.36 MPa^{-1} ($X_{Ga} = 0.027$) and decreased to 25.56 MPa^{-1} ($X_{Ga} = 0.027$) with Ga doping, indicating the synergistic effects of Ga doping and Mg alloying over the pressure sensing performance of Ga-doped MgZnO films. In general, Ga doping leads to the generation of more free electrons in MgZnO, which in turn induces higher screening effects to adversely affect the piezopotential. The trend in the enhancement of the piezotronic pressure sensor with Ga doping was consistent with the trend in d_{33} value in Fig. 4. Moreover, more force-dependent *I–V* curves (Fig. 6a, Table S5†) for stress sensitivity were obtained for the device with 1.77 at% of Ga ($X_{Ga} = 0.041$)-doped MgZnO thin film showing linear increase in the $\Delta\Phi_b$ (Fig. 6b) and linear increase in the sensitivity (Fig. 6c) with an increase in the external force (0, 0.2 and 0.5 kg). The corresponding stress sensitivity (Fig. 6d) was relatively high (31 ± 2 MPa^{-1}) at low force ($\leqq 0.5$ kg). The stress sensitivity ($\sim 1.03 \times 10^{-3}$ gf^{-1}, 31 ± 2 MPa^{-1} @ 3 V) was comparatively low as compared to the earlier publisehd reports on ZnO nanowire array (4.7×10^{-2} gf^{-1}) and the MgO layer-coated ZnO nanowire array ($\sim 10^4$).[16] However, it was unreasonable to make a direct comparison due to the significantly higher thickness of the ZnO nanowire array (~ 4 μm) as compared to the Ga:MgZnO pressure sensor (500 nm), large difference in the device design and lack of literature related to the thin film-based piezotronic pressure sensor devices. In comparison with the non-piezotronic pressure sensors such as ultrathin Au nanowires[9] (>1.14 kPa^{-1}) or flower-like $SnSe_2$ nanoplates[10] (433.22 kPa^{-1}), the stress sensitivity of the Ga:MgZnO pressure sensor was low (~ 0.03 kPa^{-1}). However, the sensor device size, design, fabrication process and dimension of Au nanowires and $SnSe_2$ nanoplates were completely different to make any valid comparison with thin film-based pressure sensors. Moreover, the minimum pressure for the sensor to detect the change in current was ~312 Pa (Fig. S5†), and the sensor was relatively stable under the application and release of stress for several cycles (Fig. S6†). The present investigation validates the combined effects of Ga doping and Mg alloying over the variation in the piezopotential, which led to a significant enhancement in the stress sensitivity of the MgZnO:Ga thin film pressure sensor. Furthermore, this unique approach could be extended using other suitable dopants to boost the pressure sensing performance of MgZnO thin films.

4. Conclusions

In summary, strong *c*-axis-oriented, high crystalline MgZnO:Ga thin films with various Ga compositions were fabricated on p-type Si (111) substrates, and the pressure sensing performance was investigated. The combined effect of Ga doping and Mg alloying led to the large enhancement of the piezopotential and subsequently the stress sensitivity of the MgZnO piezotronic pressure sensor at the optimum Ga doping concentration. XRD results described that all films had a (0002) preferential orientation with a nanorod-like columnar morphology, as investigated by SEM. Slow scan XRD results revealed that the peaks shifted depending on the amount of X_{Ga} and X_{Mg} in the films. Piezoresponse force microscopy results revealed that the MgZnO:Ga thin films with intermediate Ga concentration ($X_{Ga} = 0.027$) could achieve a higher piezoelectric coefficient (d_{33}) = 33.17 pm V^{-1}.

Conflicts of interest

There are no conflicts to declare.

Acknowledgements

This work was financially supported by the Hierarchical Green-Energy Materials (Hi-GEM) Research Center, from The Featured Areas Research Center Program within the framework of the Higher Education Sprout Project by the Ministry of Education (MOE) and the Ministry of Science and Technology (MOST 110-2634-F-006 -017) in Taiwan.

References

1 J. Zhou, Y. Gu, P. Fei, W. Mai, Y. Gao, R. Yang, G. Bao and Z. L. Wang, *Nano Lett.*, 2008, **8**, 3035–3040.
2 M. Amjadi, A. Pichitpajongkit, S. Lee, S. Ryu and I. Park, *ACS Nano*, 2014, **8**, 5154–5163.
3 X. Xiao, L. Yuan, J. Zhong, T. Ding, Y. Liu, Z. Cai, Y. Rong, H. Han, J. Zhou and Z. L. Wang, *Adv. Mater.*, 2011, **23**, 5440–5444.
4 Z. Zhang, Q. Liao, X. Zhang, G. Zhang, P. Li, S. Lu, S. Liu and Y. Zhang, *Nanoscale*, 2015, **7**, 1796–1801.
5 Z. L. Wang, *Nano Today*, 2010, **5**, 540–552.
6 Y. Hu, Y. Chang, P. Fei, R. L. Snyder and Z. L. Wang, *ACS Nano*, 2010, **4**, 1234–1240.
7 Z. Zhang, Q. Liao, X. Yan, Z. L. Wang, W. Wang, X. Sun, P. Lin, Y. Huang and Y. Zhang, *Nano Res.*, 2014, **7**, 190–198.
8 Q. Liao, M. Mohr, X. Zhang, Z. Zhang, Y. Zhang and H.-J. Fecht, *Nanoscale*, 2013, **5**, 12350–12355.
9 S. Gong, W. Schwalb, Y. Wang, Y. Chen, Y. Tang, J. Si, B. Shirinzadeh and W. Cheng, *Nat. Commun.*, 2014, **5**, 1–8.
10 W. Li, K. He, D. Zhang, N. Li, Y. Hou, G. Cheng, W. Li, F. Sui, Y. Dai and H. Luo, *ACS Appl. Energy Mater.*, 2019, **2**, 2803–2809.
11 W. Li, L. Xiong, N. Li, S. Pang, G. Xu, C. Yi, Z. Wang, G. Gu, K. Li and W. Li, *J. Mater. Chem. C*, 2019, **7**, 10179–10186.
12 M. Chen, J. Xia, J. Zhou, Q. Zeng, K. Li, K. Fujisawa, W. Fu, T. Zhang, J. Zhang and Z. Wang, *ACS Nano*, 2017, **11**, 9191–9199.
13 K. He, Y. Hou, C. Yi, N. Li, F. Sui, B. Yang, G. Gu, W. Li, Z. Wang and Y. Li, *Nano Energy*, 2020, **73**, 104743.
14 M. Chen, Z. Wang, X. Ge, Z. Wang, K. Fujisawa, J. Xia, Q. Zeng, K. Li, T. Zhang and Q. Zhang, *Matter*, 2020, **2**, 666–679.

15 S. Lu, J. Qi, Z. Wang, P. Lin, S. Liu and Y. Zhang, *RSC Adv.*, 2013, **3**, 19375–19379.
16 X. Liao, X. Yan, P. Lin, S. Lu, Y. Tian and Y. Zhang, *ACS Appl. Mater. Interfaces*, 2015, **7**, 1602–1607.
17 S. Major, A. Banerjee and K. Chopra, *Thin Solid Films*, 1983, **108**, 333–340.
18 H. Agura, A. Suzuki, T. Matsushita, T. Aoki and M. Okuda, *Thin Solid Films*, 2003, **445**, 263–267.
19 V. Bhosle, A. Tiwari and J. Narayan, *J. Appl. Phys.*, 2006, **100**, 033713.
20 T. Makino, Y. Segawa, M. Kawasaki, A. Ohtomo, R. Shiroki, K. Tamura, T. Yasuda and H. Koinuma, *Appl. Phys. Lett.*, 2001, **78**, 1237–1239.
21 L. Kukreja, S. Barik and P. Misra, *J. Cryst. Growth*, 2004, **268**, 531–535.
22 Y. Yang, C. Song, X. Wang, F. Zeng and F. Pan, *J. Appl. Phys.*, 2008, **103**, 074107.
23 J. Luo, Y. Yang, X. Zhu, G. Chen, F. Zeng and F. Pan, *Phys. Rev. B: Condens. Matter Mater. Phys.*, 2010, **82**, 014116.
24 Y. Yang, C. Song, X. Wang, F. Zeng and F. Pan, *Appl. Phys. Lett.*, 2008, **92**, 012907.
25 N. Sinha, S. Goel, A. J. Joseph, H. Yadav, K. Batra, M. K. Gupta and B. Kumar, *Ceram. Int.*, 2018, **44**(7), 8582–8590.
26 L. Kumari, W. Li, C. H. Vannoy, R. M. Leblanc and D. Wang, *Ceram. Int.*, 2009, **35**, 3355–3364.
27 Y. J. Chen, S. Brahma, C. P. Liu and J.-L. Huang, *J. Alloys Compd.*, 2017, **728**, 1248–1253.
28 J.-S. Shiau, S. Brahma, J.-L. Huang and C.-P. Liu, *Appl. Mater. Today*, 2020, **20**, 100705.
29 S. W. Shin, I. Y. Kim, G. V. Kishor, Y. Y. Yoo, Y. B. Kim, J. Y. Heo, G.-S. Heo, P. S. Patil, J. H. Kim and J. Y. Lee, *J. Alloys Compd.*, 2014, **585**, 608–613.
30 I. Y. Kim, K. Gurav, S. W. Shin, K. S. Jeon, P. Patil, J. H. Moon, D. S. Lee and J. H. Kim, *Sci. Adv. Mater.*, 2016, **8**, 610–617.
31 S.-H. Jeong, J.-H. Park and B.-T. Lee, *J. Alloys Compd.*, 2014, **617**, 52–57.
32 Dhananjay and S. Krupanidhi, *Appl. Phys. Lett.*, 2006, **89**, 082905.
33 C. Hinkle, A. Sonnet, E. Vogel, S. McDonnell, G. Hughes, M. Milojevic, B. Lee, F. Aguirre-Tostado, K. Choi and H. Kim, *Appl. Phys. Lett.*, 2008, **92**, 071901.
34 R. Kara, L. Mentar and A. Azizi, *RSC Adv.*, 2020, **10**, 40467–40479.
35 M. Ajili, M. Castagné and N. K. Turki, *Superlattices Microstruct.*, 2013, **53**, 213–222.
36 X. Wang, C. Song, D. Li, K. Geng, F. Zeng and F. Pan, *Appl. Surf. Sci.*, 2006, **253**, 1639–1643.
37 Ü. Özgür, Y. I. Alivov, C. Liu, A. Teke, M. Reshchikov, S. Doğan, V. Avrutin, S.-J. Cho and H. Morkoc, *J. Appl. Phys.*, 2005, **98**, 11.